

## Ground state of a chemically modulated Hubbard chain at half filling

Sanjay Gupta,<sup>1</sup> Shreekantha Sil,<sup>2</sup> and Bibhas Bhattacharyya<sup>3</sup>

<sup>1</sup>*TCMP Division, Saha Institute of Nuclear Physics, 1/AF-Bidhannagar, Calcutta-700 064, India*

<sup>2</sup>*Department of Physics, Vishwabharati, Shantiniketan-731 235, India*

<sup>3</sup>*Department of Physics, Scottish Church College, 1 & 3 Urquhart Square, Calcutta-700 006, India*

(Received 17 October 2000; published 12 March 2001)

We have studied the Hubbard chain with a periodic variation of the site potential for the half-filled band by using a real space renormalization group (RG) method complemented by a mean-field analysis. The ground state phase diagram shows a transition between a charge density wave (CDW) and a spin density wave (SDW). The energy gap and the local moment, as obtained from the RG, clearly identify the phase transition in agreement with the RG flow pattern. Within the mean-field approximation (MFA) the charge and spin order parameters are calculated to trace out the transition. The phase diagram obtained by the RG calculation shows excellent agreement with that obtained by the MFA especially in the weak- to intermediate-coupling region. We have also calculated the Drude weight (within the MFA) to analyze the conductivity of such a chain of *finite length*. The Drude weight also captures some interesting features of the competition between the SDW and the CDW.

DOI: 10.1103/PhysRevB.63.125113

PACS number(s): 71.10.Fd, 75.30.Fv, 71.45.Lr

### I. INTRODUCTION

The problem of electronic correlation in one dimensional (1D) and two dimensional systems has been of interest for some time. The Hubbard model with nearest-neighbor hopping and on-site electronic correlation has been considered to be the generic model in this context. This model is known to support antiferromagnetic spin density wave (SDW) order at half filling for large values of the on-site correlation. However, the effect of chemical modulation in the site potential on the SDW phase is yet to be clearly understood. An extreme example of such an effect can be found in the Hubbard model with random disorder in the site potential, a problem that already has created some interest.<sup>1</sup> In the present work we shall focus our attention on a case where the site energies in a Hubbard chain vary alternately due to a modulation in the chemical environment. This is a case that has some relevance to the  $\pi$ -bonded chains on reconstructed (111) surfaces of Si.<sup>2</sup> Very recently, such a model has been analyzed by Caprara *et al.*<sup>3</sup> by using the mean-field level of approximation. We have studied the half-filled Hubbard chain with alternating modulation in the site energy by using a real space renormalization group (RG) technique<sup>4</sup> which is expected to capture the effects of fluctuations in a low-dimensional system to a reasonable extent. Our RG results are then compared with the results of the mean-field approximation (MFA). We trace out the SDW/CDW (charge density wave) transition in the ground state of this system and observe that the variation of the site potential may result in a CDW phase even in the presence of a reasonably large value of the on-site Hubbard interaction. The local moment, as obtained from the RG, and the spin and charge order parameters, obtained from the MFA, show an interesting interplay of the two types of instability. Calculation of the Drude weight for chains of finite length also gives some insight in this respect. In Sec. II we define the Hamiltonian and explain the RG scheme. Section III describes the results obtained in

the RG, pointing out the possible limitations of the present scheme. In Sec. IV we indicate the essential steps in the calculations of the MFA and present the results obtained from it. A comparison of the RG results with the MFA results is also indicated. In Sec. V we explain the calculation of the Drude weight for chains of finite length and show the competition between the SDW and the CDW as reflected in these results. Section VI summarizes the present work.

### II. THE MODEL AND THE RG CALCULATIONS

We consider the one band Hubbard model with an alternating modulation in the site potential given by the Hamiltonian

$$H = \epsilon_A \sum_{i \in \mathcal{A}} n_i + \epsilon_B \sum_{i \in \mathcal{B}} n_i + t \sum_{\langle ij \rangle, \sigma} c_{i\sigma}^\dagger c_{j\sigma} + U_A \sum_{i \in \mathcal{A}} n_{i\uparrow} n_{i\downarrow} + U_B \sum_{i \in \mathcal{B}} n_{i\uparrow} n_{i\downarrow}, \quad (1)$$

where the bipartite 1D lattice is divided into two sublattices  $\mathcal{A}$  and  $\mathcal{B}$  consisting of the odd and even sites, respectively.  $c_{i\sigma}^\dagger$  ( $c_{i\sigma}$ ) is the creation (annihilation) operator for an electron of spin  $\sigma$  ( $=\uparrow, \downarrow$ ) in the Wannier orbital at the site  $i$ . The number operator  $n_{i\sigma} = c_{i\sigma}^\dagger c_{i\sigma}$  and  $n_i = n_{i\uparrow} + n_{i\downarrow}$ .  $t$  is the hopping integral between nearest-neighbor sites denoted by  $\langle ij \rangle$  and  $U_A$  ( $U_B$ ) is the on-site Coulomb correlation for a site belonging to the sublattice  $\mathcal{A}$  ( $\mathcal{B}$ ).  $\epsilon_A$  and  $\epsilon_B$  are the site energies on the two sublattices  $\mathcal{A}$  and  $\mathcal{B}$ , respectively.

We divide the 1D chain into cells of three sites each for implementation of the RG.<sup>4</sup> There are two types of cell, e.g.,  $ABA$  and  $BAB$ . The  $ABA$  type cell contains terminal sites belonging to the sublattice  $\mathcal{A}$  while the central site belongs to  $\mathcal{B}$ . For the  $BAB$  cell  $\mathcal{A}$  and  $\mathcal{B}$  are interchanged. The cell Hamiltonian is then diagonalized for both types of cell. Of the 64 states of the cell Hamiltonian only four low-lying

states are retained for constructing the RG recursion. The cell Hamiltonian has several conserved quantities, e.g., the total spin ( $S$ ), the  $z$  component of the total spin ( $S_z$ ), and the total number of particles ( $\nu$ ) in the cell. The Hamiltonian also possesses spin-reversal symmetry. However, the modulation in the site potential excludes the particle-hole symmetry. To obtain the half-filled ground states we retain the lowest-energy states in the subspaces with  $\{\nu=2, S=S_z=0\}$ ,  $\{\nu=3, S=1/2, S_z=\pm 1/2\}$ , and  $\{\nu=4, S=S_z=0\}$ . These four states are identified with the renormalized on-site states  $|0\rangle$ ,  $|\uparrow\rangle$ ,  $|\downarrow\rangle$ , and  $|\uparrow\downarrow\rangle$ , respectively. By this process we identify an  $ABA(BAB)$  type cell as a renormalized site belonging to the  $\mathcal{A}$  ( $\mathcal{B}$ ) sublattice on the renormalized lattice. The parameters of the Hamiltonian are then renormalized within this truncated basis set.

To renormalize the hopping matrix element  $t$  one evaluates the matrix element of  $c_\sigma^b$  between the renormalized ‘‘on-site states’’ where  $c_\sigma^b$  is the annihilation operator for spin  $\sigma$  at the boundary site  $b$  of the cell. Here we have to consider matrix elements of  $c_\sigma^b(A)$  ( $c_\sigma^b$  for the  $ABA$  type cell) and  $c_\sigma^b(B)$  ( $c_\sigma^b$  for the  $BAB$  type cell) separately. It turns out that

$$\begin{aligned} {}_{ABA}\langle \nu=2, S=S_z=0 | c_\uparrow^b(A) | \nu=3, S=S_z=\frac{1}{2} \rangle_{ABA} &= \lambda_1(A), \\ {}_{ABA}\langle \nu=3, S=-S_z=\frac{1}{2} | c_\uparrow^b(A) | \nu=4, S=S_z=0 \rangle_{ABA} &= \lambda_2(A), \\ {}_{BAB}\langle \nu=2, S=S_z=0 | c_\uparrow^b(B) | \nu=3, S=S_z=\frac{1}{2} \rangle_{BAB} &= \lambda_1(B), \end{aligned} \quad (2)$$

$${}_{BAB}\langle \nu=3, S=-S_z=\frac{1}{2} | c_\uparrow^b(B) | \nu=4, S=S_z=0 \rangle_{BAB} = \lambda_2(B),$$

where the subscript  $ABA(BAB)$  refers to states of the  $ABA$  ( $BAB$ ) type cell. Here  $\lambda_1(A) \neq \lambda_2(A)$  and  $\lambda_1(A) \neq \lambda_2(A)$  due to the lack of particle-hole symmetry. However, the matrix element for the  $c_\uparrow^b$ 's will have the same magnitude as those for the  $c_\downarrow^b$ 's due to the spin-reversal symmetry. We therefore make an approximation by defining  $\lambda(A) = \sqrt{|\lambda_1(A)\lambda_2(A)|}$  and  $\lambda(B) = \sqrt{|\lambda_1(B)\lambda_2(B)|}$  so that we can identify

$$c_\sigma^b(\Gamma) = \lambda(\Gamma) c'_\sigma(\Gamma), \quad \Gamma = A, B. \quad (3)$$

This leads to the effective renormalized hopping

$$t' = \lambda(A)\lambda(B)t. \quad (4)$$

Such approximations for finding the renormalized hopping have already been used.<sup>5,6</sup> The present approximation seems reasonable because different approximations for the  $\lambda$ 's [e.g.,  $\lambda(\Gamma) = \sqrt{|\lambda_1(\Gamma)\lambda_2(\Gamma)|}$  or  $\lambda(\Gamma) = \frac{1}{2}(|\lambda_1(\Gamma)| + |\lambda_2(\Gamma)|)$  with  $\Gamma = A, B$ ] do not alter the final results appreciably. Moreover, if we allow the different values of  $\lambda_1(A)[\lambda_1(B)]$  and  $\lambda_2(A)[\lambda_2(B)]$  we are left with four distinct hopping amplitudes corresponding to four density dependent hopping processes. One could use the generalized Hubbard model with four hopping processes and, as we have checked, such a generalization does not markedly alter the results at the cost of enlarging the parameter space.

Renormalization of the on-site quantities is straightforward.<sup>4</sup>

$$\begin{aligned} U'_\Gamma &= E_4(\Gamma) + E_2(\Gamma) - 2E_3(\Gamma), \\ \epsilon'_\Gamma &= E_3(\Gamma) - E_2(\Gamma) \quad \text{where } \Gamma = A, B. \end{aligned} \quad (5)$$

Here, the primed quantities refer to the renormalized values.  $E_4$ ,  $E_3$ , and  $E_2$  refer to the lowest energies in the subspaces corresponding to  $\nu=4, 3$ , and  $2$ , respectively. We start with  $U_A = U_B = U$  and observe that  $U'_A = U'_B$  at all subsequent iterations.

Hence one can calculate the ground state energy per site ( $E_0$ ) by computing the sum

$$E_0 = \frac{1}{2} \sum_{n=1}^{\infty} \frac{[E_2^{(n)}(A) + E_2^{(n)}(B)]}{3^n},$$

where  $n$  denotes the  $n$ th stage of iteration in the summation. We can also calculate the local moment  $L_0$  defined by

$$L_0 = \frac{3}{4}(n_\uparrow - n_\downarrow)^2.$$

In the absence of particle-hole symmetry this leads to the recursion relation

$$L_0 = a + bL'_0 + cP',$$

where  $P = (n_\uparrow + n_\downarrow)(n_\uparrow + n_\downarrow - 1)$  obeys a recursion relation of the form

$$P = d + eL'_0 + fP'$$

with  $a, b, c, d, e$ , and  $f$  quantities obtained from the matrix elements of  $L_0$  and  $P$  between the truncated basis states of the cell Hamiltonian. The operators  $L_0$  and  $P$  are considered for the central site of the cell to minimize the boundary effects.<sup>4</sup> In spite of having two types of cell ( $ABA$  and  $BAB$ ) we obtain the same value for  $L_0$  for both cells.

### III. THE RESULTS OF THE RG CALCULATIONS

We start our iteration with  $\epsilon_A = 0$ ,  $\epsilon_B = \epsilon \geq 0$ , and  $U_A = U_B = U \geq 0$ . As we mentioned earlier, in this particular problem we obtain  $U'_A = U'_B$  at all stages of iteration;  $\epsilon'_A$  and  $\epsilon'_B$ , however, go on changing with each iteration. The phase transition from the CDW to the SDW phase can be identified by plotting the RG flow patterns in the ‘‘effective’’ parameter space  $\{U/t, (\epsilon_B - \epsilon_A)/t\}$ . The line of repulsion of the flow lines indicates the phase boundary (Fig. 1). Starting from any point above this line the RG flow tends to go to the fixed point  $\{0, \infty\}$ , indicating a CDW phase, while any point below the boundary flows to  $\{\infty, 0\}$ , which is the SDW fixed point. There is, however, a noticeable difference in the flow patterns in these two regimes. In the CDW regime the flow lines approach the  $\{0, \infty\}$  fixed point in a monotonic fashion while in the SDW sector the flow lines appear to deviate away from the  $U/t$  axis before finally bending toward the  $\{\infty, 0\}$  fixed point. This perhaps is a signature of the residual CDW fluctuations competing with the SDW ordering in this sector. Such a behavior is also observed in our analysis of the order parameters in the MFA. This effect was also noted in Ref. 3. The flow diagram also shows that the metallic

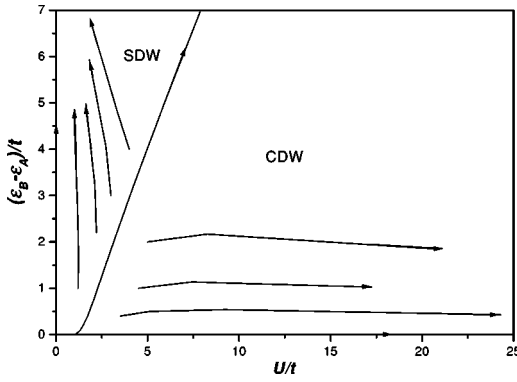


FIG. 1. RG flow diagram for the half-filled band Hubbard model with alternating site potentials in one dimension. For the sake of simplicity an “effective” parameter space  $\{(\epsilon_B - \epsilon_A)/t, U/t\}$  is chosen. We always start with  $\epsilon_A = 0$  with  $\epsilon_B = \epsilon_B - \epsilon_A$ . The arrows show that the  $\{0,0\}$  point is a singular one. The tendency for the flow lines in the SDW sector to go over to  $\{\infty, 0\}$  is not clearly seen from the present diagram because the turning off takes place at much higher values of  $U/t$  than those shown on the plot.

fixed point  $\{0,0\}$  is a singular one and, therefore, the present model is always insulating for the half-filled band in a 1D system.

The phase boundary (Fig. 2) identified from the plot of the flow lines can further be verified to be the line along which the energy gap vanishes. The energy gap  $\Delta$  between the first excited state and the ground state is plotted against  $U/t$  for different values of  $\epsilon_B - \epsilon_A$  (Fig. 3). For a given value of  $\epsilon_B - \epsilon_A$  the energy gap decreases first with increasing  $U/t$  and vanishes for a critical value  $(U/t)_c$  of  $U/t$ . For  $U/t=0$  the system becomes a CDW insulator with a tendency to predominantly occupy the sites with lower site potential (i.e.,  $\mathcal{A}$  sites since  $\epsilon_A < \epsilon_B$ ) while avoiding the others. As  $U$  increases it becomes energetically favorable to break up the double occupancies and, therefore, the CDW energy gap is reduced. This scenario persists up to  $(U/t)_c$  where the critical competition between the electronic correlation and the modulation of the site potential makes the spectrum gapless.

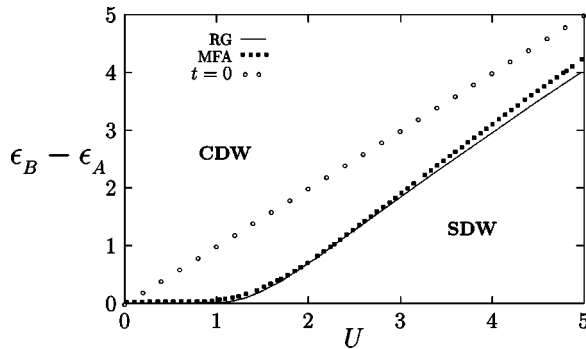


FIG. 2. The phase diagram of the half-filled band Hubbard model with alternating site potentials in one dimension. The phase boundary obtained in the RG scheme is compared with that obtained by the MFA. To draw this phase diagram in the  $\{\epsilon_B - \epsilon_A, U\}$  space we always started from  $\epsilon_A = 0$  with  $\epsilon_B = \epsilon_B - \epsilon_A$  and  $t = 1.0$ . The phase boundary for the atomic limit  $t = 0$  is also shown.

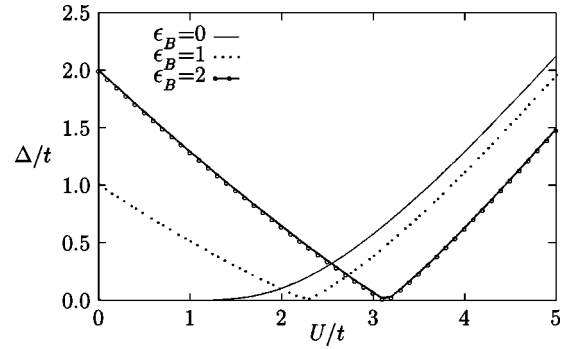


FIG. 3. The energy gap  $\Delta$  scaled by the hopping integral  $t$  is plotted against  $U/t$  for different values of  $\epsilon_B = \epsilon_B - \epsilon_A$  with  $\epsilon_A = 0$ . For  $\epsilon_B = 0$ ,  $\Delta$  is always nonzero except for  $U/t = 0$ . For  $\epsilon_B \neq 0$  the gap vanishes at a certain value of  $U/t$  which marks the CDW/SDW transition.

However, the gap opens up again with increasing values of  $U/t$  as the antiferromagnetic SDW phase sets in. A plot of the  $(U/t)_c$ 's against  $\epsilon_B - \epsilon_A$  generates the same phase boundary as obtained from the RG flow. It is interesting to note that the exact value of the energy gap ( $= \epsilon_B - \epsilon_A$ ) for the CDW insulating phase for  $U/t = 0$  is reproduced in the RG scheme.

The local moment  $L_0$  plotted against  $U/t$  (Fig. 4) for a fixed value of  $\epsilon_B - \epsilon_A$  also captures the transition between the CDW and SDW states. In the CDW phase the tendency to form pairs is more pronounced for the half-filled band; therefore,  $L_0$  assumes a low value. However,  $L_0$  goes on increasing as the pairs tend to break up with the increase of  $U/t$ . In the SDW sector the rise of  $L_0$  is faster compared to that in the CDW regime, as one should expect on physical grounds. The discontinuity in the slope of the local moment (clearly visible in the plot of  $L_0$  for higher values of  $\epsilon_B - \epsilon_A$ ) marks the CDW/SDW transition.

The ground state energy per site  $E_0$  varies smoothly with  $U/t$  across the CDW/SDW transition (Fig. 5).  $E_0$  calculated from the RG, however, gives an upper bound<sup>4</sup> to the exact

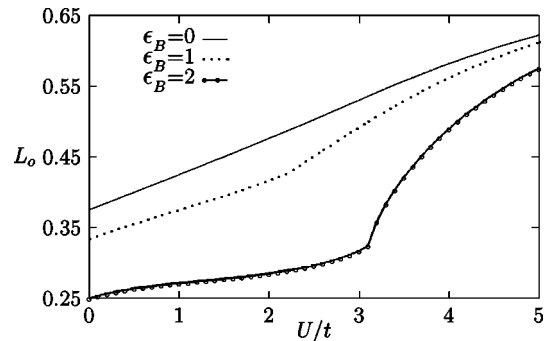


FIG. 4. The local moment  $L_0$  is plotted against  $U/t$  for different values of  $\epsilon_B = \epsilon_B - \epsilon_A$  with  $\epsilon_A = 0$ . For  $\epsilon_B = 0$ ,  $L_0$  increases monotonically while for  $\epsilon_B \neq 0$  there appears a discontinuity in the slope of  $L_0$  at the point of transition. This becomes evident if Fig. 3 is compared with the present figure. The magnitude of the discontinuity in the slope increases with the increase of  $\epsilon_B$  and, therefore, it is very hard to detect this effect for smaller values of  $\epsilon_B$ .

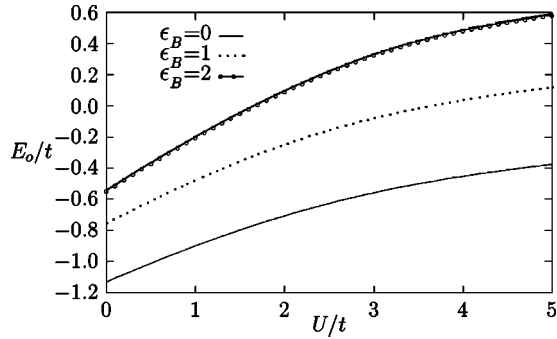


FIG. 5. Plot of the ground state energy per site  $E_0$  (obtained from the RG) scaled by the hopping integral  $t$  against  $U/t$  for different values of  $\epsilon_B = \epsilon_B - \epsilon_A$  with  $\epsilon_A = 0$ .

energy and converges to the exact value  $[(\epsilon_B + \epsilon_A)/2]$  as  $U/t \rightarrow \infty$ .

It should be noted that the approximations introduced by the truncation of the basis set of the cell Hamiltonian may give rise to some trouble in the strong-coupling regime of the parameter space of the present model. The effect of truncation of the basis set and the approximation introduced by the small size of the cells are well known for the present RG scheme<sup>4,7,8</sup> although these effects do not mask the essential physical properties of a system of correlated electrons.<sup>4,9-11</sup> In the present model, however, the competition between the modulation of the site potential and the Hubbard correlation makes the situation a difficult one. Since we are considering *two types of cell ABA and BAB*, the lowest-lying states retained in two neighboring cells may have considerably different energies in the strong-coupling regime  $\{(\epsilon_B - \epsilon_A)/t \gg 1, U/t \gg 1\}$ . As a result of this, the energy scale chosen for the retained states in one type of cell may be such that some of the discarded states in the other type of cell may have energies falling within this range; this, of course, may result in some inaccuracies in the results. In our case we find a signature of this feature in the strong-coupling regime of the phase diagram. For very large values of  $U/t$  the phase boundary is expected to merge with the line  $U = \epsilon_B - \epsilon_A$  (obtained in the atomic limit). However, the convergence of the phase boundary obtained in the RG with that of the atomic limit is much slower (almost undetectable in Fig. 2) than that of the phase boundary obtained in the MFA. This inadequacy of the present RG calculation may be overcome by using a scheme<sup>12</sup> where more levels can be retained at each iteration. A density matrix RG scheme<sup>7</sup> may also lead to a better result.

#### IV. THE MEAN-FIELD CALCULATIONS

We now attempt a mean-field analysis<sup>13</sup> of the present model. We define the following parameters in terms of the expectation values of the number operators at sites belonging to different sublattices:

$$\begin{aligned} n &= n_{A\uparrow} + n_{A\downarrow} + n_{B\uparrow} + n_{B\downarrow}, \\ m &= (n_{A\uparrow} - n_{A\downarrow}) - (n_{B\uparrow} - n_{B\downarrow}), \end{aligned} \quad (6)$$

$$c = (n_{A\uparrow} + n_{A\downarrow}) - (n_{B\uparrow} + n_{B\downarrow}).$$

Here  $n_{A\sigma}$  and  $n_{B\sigma}$  (with  $\sigma = \uparrow, \downarrow$ ) are the expectation values of  $n_{i\sigma}$  for  $i \in \mathcal{A}$  and  $i \in \mathcal{B}$ , respectively.

Now the Hubbard interaction term is decoupled in terms of the parameters defined above. This leads to the mean-field decoupled Hamiltonian,

$$\begin{aligned} H &= \left( \epsilon_A + \frac{U}{4}(c-m) \right) \sum_{i \in \mathcal{A}} n_{i\uparrow} + \left( \epsilon_B - \frac{U}{4}(c-m) \right) \sum_{i \in \mathcal{B}} n_{i\uparrow} \\ &+ \left( \epsilon_A + \frac{U}{4}(c+m) \right) \sum_{i \in \mathcal{A}} n_{i\downarrow} + \left( \epsilon_B - \frac{U}{4}(c+m) \right) \sum_{i \in \mathcal{B}} n_{i\downarrow} \\ &+ t \sum_{\langle ij \rangle, \sigma} c_{i\sigma}^\dagger c_{j\sigma} + \frac{UN}{16}(n^2 - c^2 + m^2), \end{aligned} \quad (7)$$

where  $N$  is the number of sites in the chain.  $H$  can be readily diagonalized by a canonical transformation<sup>13</sup> to yield the ground state energy per site for the half-filled band,

$$\begin{aligned} E_0 &= \frac{1}{2} \left( \epsilon_A + \epsilon_B + \frac{U}{2} \right) + \frac{1}{16} U(1 + m^2 - c^2) - \frac{1}{2N} \sum_{j=0}^{N/2-1} \\ &\times \left[ \sqrt{\left( \epsilon_A - \epsilon_B + \frac{U}{2}(c-m) \right)^2 + 8t^2(1 + \cos 2k_j)} \right. \\ &\left. + \sqrt{\left( \epsilon_A - \epsilon_B + \frac{U}{2}(c+m) \right)^2 + 8t^2(1 + \cos 2k_j)} \right], \end{aligned} \quad (8)$$

as a function of  $c$  and  $m$  for given values of  $U$ ,  $t$ ,  $\epsilon_B$ , and  $\epsilon_A$  for even values of the chain length  $N$ . The  $k_j$ 's are given by

$$k_j = \frac{2\pi j}{N} \quad \text{with } j = 0, 1, \dots, N/2 - 1.$$

However, the choice of even values of  $N$  does not matter as we let  $N$  approach the thermodynamic limit, i.e.,  $N \rightarrow \infty$ , keeping the filling constant.

Now, minimization of the ground state energy with respect to the spin and charge order parameters,  $m$  and  $c$ , respectively, determines the unique values of  $c$  and  $m$  and the energy per site in the ground state. This amounts to solving

$$\frac{\partial E_0}{\partial c} = 0 \quad \text{and} \quad \frac{\partial E_0}{\partial m} = 0.$$

This leads to the two coupled equations

$$\begin{aligned} c &= \frac{2}{N} \sum_{j=0}^{N/2-1} \frac{(\epsilon_B - \epsilon_A) - (U/2)(c-m)}{\sqrt{[\epsilon_A - \epsilon_B + (U/2)(c-m)]^2 + 8t^2(1 + \cos 2k_j)}} \\ &+ \frac{2}{N} \sum_{j=0}^{N/2-1} \frac{(\epsilon_B - \epsilon_A) - (U/2)(c+m)}{\sqrt{[\epsilon_A - \epsilon_B + (U/2)(c+m)]^2 + 8t^2(1 + \cos 2k_j)}}, \end{aligned} \quad (9)$$

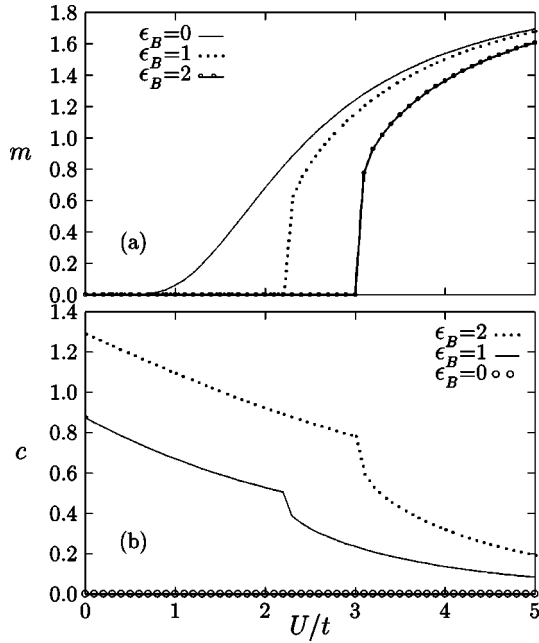


FIG. 6. Plots of (a) the spin order parameter  $m$  and (b) the charge order parameter  $c$  against  $U/t$  for different values of  $\epsilon_B = \epsilon_B - \epsilon_A$  with  $\epsilon_A = 0$ . Across the transition point the order parameters show discontinuities, the magnitudes of which increase with increasing values of  $\epsilon_B$ .

$$m = \frac{2}{N} \sum_{j=0}^{N/2-1} \frac{(\epsilon_B - \epsilon_A) - (U/2)(c - m)}{\sqrt{[\epsilon_A - \epsilon_B + (U/2)(c - m)]^2 + 8t^2(1 + \cos 2k_j)}} - \frac{2}{N} \sum_{j=0}^{N/2-1} \frac{(\epsilon_B - \epsilon_A) - (U/2)(c + m)}{\sqrt{[\epsilon_A - \epsilon_B + (U/2)(c + m)]^2 + 8t^2(1 + \cos 2k_j)}}, \quad (10)$$

where these two equations are solved self-consistently to find  $c$ ,  $m$ , and hence  $E_0$ .

The charge order parameter  $c$  assumes a high value in the CDW sector and gradually decreases with increasing  $U/t$  (Fig. 6). It suddenly jumps down across the CDW/SDW transition point at a value  $(U/t)_c$  of  $U/t$ . Then it slowly goes on decreasing with increasing  $U/t$ . On the other hand, the spin order parameter is perfectly zero in the CDW phase and suddenly jumps up to a finite value across the transition point  $(U/t)_c$ . In the SDW phase  $m$  gradually increases to the maximum possible value [according to our definitions (6)  $c$  and  $m$  can vary between 0 and 2]. Plots of  $c$  and  $m$  show that an increase in  $\epsilon_B - \epsilon_A$  enhances  $c$  and suppresses the value of  $m$  as it favors charge ordering over antiferromagnetic instability. The values of  $(U/t)_c$  for different  $\epsilon_B - \epsilon_A$  thus obtained give rise to the phase diagram within the MFA (Fig. 2). It is interesting to note that the phase boundary obtained in the MFA scheme agrees nicely with that obtained in the RG especially in the regime of weak to intermediate coupling. It seems, therefore, that the agreement between the results obtained in two widely different schemes occurs because the approximations involved in these calculations do not seriously affect the results (as far as the CDW/SDW

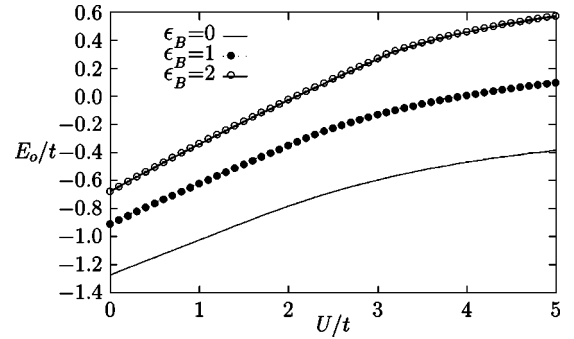


FIG. 7. Plot of the ground state energy per site  $E_0$  (obtained from the MFA) scaled by the hopping integral  $t$  against  $U/t$  for different values of  $\epsilon_B = \epsilon_B - \epsilon_A$  with  $\epsilon_A = 0$ .

transition is concerned) for the present model in the weak- to intermediate-coupling regime of the parameter space. However, we find a departure of the phase boundary obtained in the RG from that obtained in the MFA in the strong-coupling region of the parameter space (Fig. 2). Here we find a gradual bending of the mean-field phase boundary toward the transition line ( $\epsilon_B - \epsilon_A = U$ ) obtained in the atomic limit ( $t = 0$ , for which a transition occurs from a CDW to a singly occupied paramagnetic phase). This feature must show up as  $(\epsilon_B - \epsilon_A)/t \rightarrow 0$  and  $U/t \rightarrow 0$  and its absence in the RG result points out some limitation of the present RG scheme in the strong-coupling region as noted in Sec. III.

One interesting feature showing up in Fig. 6 is that the spin order parameter  $m$  vanishes in the entire CDW region while in contrast to this the charge order parameter  $c$  does not vanish identically in the SDW region. For  $U/t$  values very close to  $(U/t)_c$   $c$  has an appreciable value (although much smaller than that of  $m$ ) and goes on gradually decreasing with increasing  $U/t$ . This shows that there exists a crucial competition between the charge and spin ordering instabilities near the transition line inside the SDW region and not within the CDW sector. The signature of this effect has already been noted in our previous discussion of the RG flow diagram. This effect was previously observed in Ref. 3. In the next section we shall again address this issue in the context of calculation of the Drude weight for finite chains.

The ground state energy per site  $E_0$  calculated from the MFA scheme (Fig. 7) becomes exact for  $t = 0$  and for  $U = 0$ . It turns out that the value of  $E_0$  obtained in the MFA calculation is significantly lower than that obtained in the RG scheme in the weak- to intermediate-coupling region. However, in the strong-coupling regime the MFA result (for  $E_0$ ) quickly approaches the RG result.

## V. THE DRUDE WEIGHT AND THE CONDUCTIVITY

In order to study the conductivity of the present model on a finite chain one can study the response to a small static electric field in terms of the Drude weight.<sup>14,15</sup> We take a finite chain of  $N$  sites (with even  $N$ ) in the form of a ring that is threaded by a flux  $\Phi$  (in units of the basic flux quantum  $\phi_0 = \hbar c/e$ ). This modifies the hopping term in the Hamiltonian (1) by a phase factor involving the vector potential

$\phi = \Phi/N$ . The hopping term appears as

$$t \sum_{\sigma, i=1}^N (c_{i\sigma}^\dagger c_{i+1\sigma} e^{i\phi} + c_{i+1\sigma}^\dagger c_{i\sigma} e^{-i\phi}),$$

where the lattice spacing is set equal to unity. As originally noted by Kohn,<sup>16</sup> the Drude weight  $D$  can be calculated from

$$D = \frac{1}{N} \left[ \frac{\partial^2 E(\phi)}{\partial \phi^2} \right]_{\phi=0}, \quad (11)$$

where  $E(\phi)$  is the ground state energy of the  $N$ -site ring threaded by the flux  $\Phi = N\phi$ .

The ground state energy  $E(\phi)$  has been calculated within the MFA scheme as discussed in Sec. IV.  $E_0(\phi) = E(\phi)/N$ , the energy per site in the presence of the threading flux  $\Phi$ , can be calculated from the expression (8) for  $E_0$  together with Eqs. (9) and (10) (arising from minimization of the energy with respect to  $c$  and  $m$ ) with  $k_j$  replaced by  $k_j + \phi$ .

The plot of the Drude weight as a function of  $U/t$  for different values of the system size  $N$  (Fig. 8) shows that the conductivity goes down to zero for the thermodynamic limit; this indicates that the system is insulating in this limit. However, for small enough system size there is a possibility of having a finite (maybe small) value of  $D$ . Figure 8(a) shows that the SDW phase (for  $\epsilon_B - \epsilon_A = 0$ ) supports a finite value of  $D$  for small system sizes for smaller values of  $U/t$  where the SDW fluctuation is weak. For large values of  $U/t$  the conductivity goes to zero owing to an insulating antiferromagnetic order.  $D$  suddenly drops down to zero at a definite value of  $U/t$ , which shifts toward  $U/t=0$  with increasing  $N$ . For  $\epsilon_B - \epsilon_A \neq 0$ ,  $D$  is almost zero inside the CDW region owing to the insulating charge order. This points out the basic difference between the SDW and CDW fluctuations in regard to the conduction properties. This competing nature of these two types of instability is revealed in Figs. 8(b) and 8(c).  $D$  suddenly jumps up across the transition point  $(U/t)_c$  in going from the CDW to the SDW phase and then gradually falls down to zero. The sudden increase in  $D$  is triggered by the onset of the SDW instabilities; however, the nonzero value of  $D$  is less sustained due to the residual CDW fluctuations inside the SDW sector. As  $\epsilon_B - \epsilon_A$  increases the value of  $D$  around  $(U/t)_c$  decreases, because with the enhancement of the chemical modulation the value of  $(U/t)_c$  also increases and consequently both the spin- and charge-ordering fluctuations are strengthened enough to suppress the conductivity. It is also interesting to note that for a fixed value of  $\epsilon_B - \epsilon_A$  the value of  $(U/t)_c$  decreases with increasing  $N$ , as evident from the plots of the Drude weight. This is because the enhanced hopping effect smears out the effect of modulation in the site potential with a tendency to disfavor the charge order.

The competing nature of the SDW and CDW instabilities is further shown in the plot of the Drude weight against the system size  $N$  for fixed  $U/t$  and  $\epsilon_B - \epsilon_A$  (Fig. 9). We find that  $D$  falls sharply with increasing  $N$  up to a certain value of  $N$  and then suddenly jumps to a large value, and then again decreases with  $N$  (for  $U/t=1.23$  and  $\epsilon_B=0.1, \epsilon_A=0$ ). We

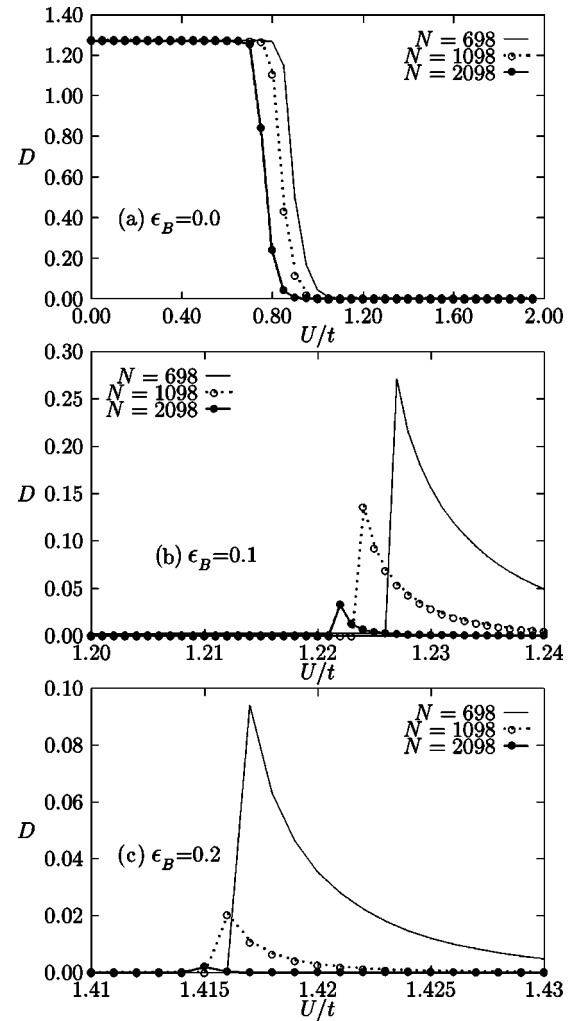


FIG. 8. Plot of the Drude weight  $D$  against  $U/t$  for different  $N$  for  $\epsilon_B = \epsilon_B - \epsilon_A$  with  $\epsilon_A = 0$ : (a)  $\epsilon_B = 0.0$ , (b)  $\epsilon_B = 0.1$ , and (c)  $\epsilon_B = 0.2$ . Across the transition (for  $\epsilon_B > 0$ )  $D$  jumps up and the transition point is seen to shift toward lower values of  $U/t$  for increasing system size. The length of the chain  $N$  is chosen not to be a multiple of 4 because in this case there appears a discontinuity in the slope of  $E(\phi)$  across  $\phi=0$  (Refs. 14,15) which prevents the application of Eq. (11).

have already noted from Fig. 8 that  $(U/t)_c$  increases with decreasing  $N$  and, therefore, at a fixed value of  $U/t$  we can enter SDW ordering from the CDW ordering just by increasing  $N$ . We can find a fixed value of  $N$  (say  $N_0$ ) for which this particular  $U/t$  is  $(U/t)_c$ . For  $N < N_0$  we surely find CDW ordering while  $N > N_0$  gives a SDW sector. This gives rise to the enhancement of  $D$  at  $N = N_0$ . Moreover, we note that for a higher value of  $U/t$  (for which  $N_0$  is much smaller than the lowest  $N$  included in Fig. 9) there is a gradual, monotonic decrease of  $D$  with  $N$ , which is expected in the SDW sector. Now comparing these two graphs (with different  $U/t$ ) we find that the Drude weight diminishes with an increase in  $U/t$  in the region where  $N > N_0$  ( $N_0$  corresponding to  $U/t = 1.23$ ). In this region, both the curves correspond to SDW ordering. Hence a decrease in  $D$  is expected with the strengthening of the antiferromagnetic fluctuations for larger

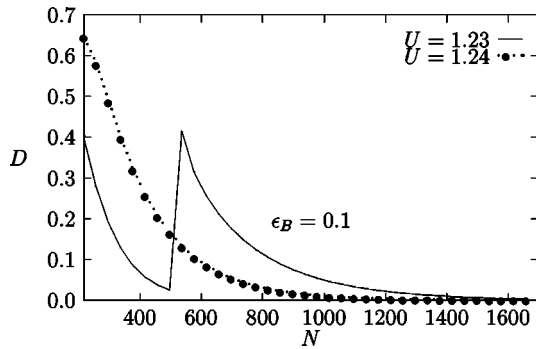


FIG. 9. Plot of the Drude weight  $D$  against  $N$  for different  $U$  (taking  $t=1.0$ ). For  $U/t=1.23$  the curve dips down at  $N=N_0$ , for which  $(U/t)_c=1.23$ .  $N_0$  for  $U/t=1.24$  falls beyond (smaller  $N$ ) the graph.

values of  $U$ . As a result of this the curve with the lower value of  $U/t$  lies above the curve with the higher  $U/t$ . However, the reverse is found below  $N_0$  where the smaller value of  $U/t$  corresponds to CDW ordering while the curve for higher  $U/t$  still corresponds to the SDW sector. It is interesting to note how the CDW fluctuation *suppresses the conductivity* such that  $D$  increases in spite of the increase of the repulsive interaction  $U$  in this region.

## VI. CONCLUSION

Summarizing, we have studied a 1D model of electrons interacting via an on-site Hubbard correlation and moving in a chemically modulated lattice of alternating site potentials. We have primarily used a real space RG scheme suitably adapted for the present problem; this technique is known to retain to a great extent the effects of fluctuations of low-dimensional systems. This is supplemented by a MFA and

calculation of the conductivity for finite-sized chains. Our study, for the half-filled band, shows a transition from the CDW to the SDW phase. The phase diagram obtained by the RG calculations agrees nicely with that obtained in the MFA for the weak- to intermediate-coupling regions in the phase diagram. The agreement between the results obtained in two different approximation schemes lends some support to the results obtained in this regime. Moreover, these two techniques appear to be complementary to each other for the present problem. The local moment calculated from the RG marks the transition by a discontinuity in its slope while the mean-field order parameters jump discontinuously across the transition. The energy gap, as estimated from the RG calculations, also vanishes at the phase boundary. However, the MFA captures in a better way the bending of the phase boundary toward that of the atomic limit of the model. This apparent inefficacy of the present RG scheme, however, was already anticipated in terms of the effect of truncation of the basis in the presence of very strong modulation in the chemical environment. The Drude weight shows that the present model is always insulating in the thermodynamic limit and it is in agreement with the RG flow. For small systems the conductivity assumes a nonzero value across the transition from the CDW to the SDW sector; this is due to the onset of weak SDW fluctuations which favor conduction compared to the charge ordering instabilities. On the SDW side of the transition the interplay between the spin and charge ordering makes the Drude weight less sustained. This feature, also evident from the mean-field order parameters and the trends in the RG flow lines, is in agreement with a previous result for this model.<sup>3</sup> It seems interesting at this point to investigate this model in higher dimensions and also for finite temperatures. The present study indicates that the MFA scheme may be a reliable tool for such studies for this model. The effect of the band filling will also be of great interest.

<sup>1</sup>A. W. Sandvik and D. J. Scalapino, Phys. Rev. B **47**, 10 090 (1993); A. W. Sandvik, D. J. Scalapino, and P. Henelius, *ibid.* **50**, 10 474 (1994).

<sup>2</sup>M. Lannoo and G. Allan, Solid State Commun. **47**, 153 (1983).

<sup>3</sup>S. Caprara, M. Avignon, and O. Navarro, Phys. Rev. B **61**, 15 667 (2000).

<sup>4</sup>J. E. Hirsch, Phys. Rev. B **22**, 5259 (1980); C. Dasgupta and P. Pfeuty, J. Phys. C **14**, 717 (1981).

<sup>5</sup>M. Ma, Phys. Rev. B **26**, 5097 (1982).

<sup>6</sup>B. Bhattacharyya and S. Sil, Phys. Lett. A **180**, 299 (1993).

<sup>7</sup>S. R. White, Phys. Rev. Lett. **69**, 2863 (1992); Phys. Rev. B **48**, 10 345 (1993).

<sup>8</sup>B. Bhattacharyya and S. Sil, Phys. Lett. A **210**, 129 (1996); Phys. Rev. B **57**, 11 831 (1998).

<sup>9</sup>B. Bhattacharyya and S. Sil, J. Phys.: Condens. Matter **7**, 6663 (1995); **8**, 911 (1996); S. Sil and B. Bhattacharyya, Phys. Rev. B **54**, 14 349 (1996).

<sup>10</sup>B. Bhattacharyya and G. K. Roy, J. Phys.: Condens. Matter **7**, 5537 (1995).

<sup>11</sup>B. Bhattacharyya and S. Sil, J. Phys.: Condens. Matter **11**, 3513 (1999).

<sup>12</sup>S.-T. Chui and J. W. Bray, Phys. Rev. B **18**, 2426 (1978).

<sup>13</sup>D. Cabib and E. Callen, Phys. Rev. B **12**, 5249 (1975).

<sup>14</sup>R. M. Fye *et al.*, Phys. Rev. B **44**, 6909 (1991); D. J. Scalapino, S. R. White, and Z. Shoucheng, *ibid.* **47**, 7995 (1993).

<sup>15</sup>G. Bouzerar, D. Poilblanc, and G. Montambaux, Phys. Rev. B **49**, 8258 (1994).

<sup>16</sup>W. Kohn, Phys. Rev. **133**, A171 (1964).